Resolution and Micro-Doppler Effect in Bi-ISAR System

Deng Dong-hu*[①] Zhang Qun[①] Luo Ying[①] Li Song[②] Zhu Ren-fei[①]
[①](*Institute of Information and Navigation, Air Force Engineering University, Xi'an* 710077, *China*)
[②](*Institute of Air and Missile Defense, Air Force Engineering University, Xi'an* 710051, *China*)

Abstract: Compared to the monostatic radar, bistatic radar has many special characteristics because of its spatial complexity. Bistatic Inverse Synthetic Aperture Radar (Bi-ISAR) can be employed as a radar imaging tool for obtaining non-cooperative target images. In this study, we first analyze the range and azimuth resolution of a Bi-ISAR system. To analyze this azimuth resolution and its spatial-variety characteristic, a definition called con-Doppler bandwidth is introduced, which helps overcome the difficulty of the target's viewing angle diversity calculation. Then, a detailed investigation is conducted to study the micro-Doppler effect caused by the vibration and the rotation of the target in the Bi-ISAR system. By comparing the difference in the micro-Doppler effect between the Bi-ISAR system and the Mono-ISAR system, we modify the extended Hough transform to extract the real micro-motion features of the targets. Finally, we provide some simulation results to validate the theoretical derivation and to illustrate the effectiveness of the proposed method.

Key words: Bi-static radar; Inverse Synthetic Aperture Radar (ISAR); Resolution; Micro-Doppler effect; Hough transform
CLC index: TN957
DOI: 10.3724/SP.J.1300.2013.13039

双基地 ISAR 系统中分辨率分析及微多普勒效应研究

邓冬虎[①] 张 群[①] 罗 迎[①] 李 松[②] 朱仁飞[①]
[①](空军工程大学信息与导航学院 西安 710077)
[②](空军工程大学防空反导学院 西安 710051)

摘 要：由于空间的高度复杂性，双基地雷达系统中目标微动产生的微多普勒信息与单基地体制雷达有较大区别。双基地逆合成孔径雷达（ISAR）可以看做获得非协作目标图像的雷达成像工具。该文首先分析了双基地 ISAR 系统的 2 维分辨率，并提出了合多普勒带宽的概念来分析方位分辨率和它的空变性。然后，详细研究了双基地 ISAR 系统中旋转和振动所产生的微多普勒效应。基于双基地 ISAR 系统和单基地 ISAR 系统微多普勒效应的不同，该文提出了一种扩展 Hough 变换来提取目标的实际微动特征。最后，通过仿真实验验证了结论的正确性和有效性。

关键词：双基地雷达；逆合成孔径雷达；分辨率；微多普勒效应；Hough 变换
中图分类号：TN957 **文献标识码**：A **文章编号**：2095-283X(2013)02-0152-12

1 Introduction

Bi-static Synthetic Aperture Radar (Bi-SAR) system, whereby the transmitter and the receiver are mounted on two separate platforms, has aroused great attentions in recent years because of its special advantage compared to the monostatic imaging radar[1−4]. As a radar imaging tool for obtaining non-cooperative target images, the Bi-static Inverse Synthetic Aperture Radar (Bi-ISAR) has also progressed in the last years[5]. As it is known to all, ISAR images could be obtained by using wide bandwidth pulses and by coherently integrating the received target echoes. In the conventional ISAR system, it is necessary for the target to change its viewing angle with respect to the radar to obtain higher azimuth resolution. In some instances, especially when the target is

Manuscript received April 7, 2013; revised June 6, 2013.
Published online June 14, 2013.
Supported by the National Natural Science Foundation of China (No. 61172169), and the National Natural Science Foundation for Young Scientist of China (No. 61201369, 61102109).
*Communication author: Deng Dong-hu.
E-mail: dengdonghu@163.com.

moving along the radar Line Of Sight (LOS), the viewing angle is not sufficient to form an ISAR image in the conventional ISAR system. The application of Bi-ISAR geometries, which provide adequate viewing angle diversity of the target, can help overcome this problem. In addition, Bi-ISAR has many other advantages like those shown in Refs. [1–3, 6]. However, because of the spatial complexity of Bi-ISAR system, some characteristics of moving targets such as micro-Doppler effect in Bi-ISAR system are different from those in the conventional ISAR system.

The micro-Doppler features can be regarded as a unique signature of an object with movements and provide additional information for the classification, recognition, and identification of the object[7−9]. On the other hand, the existence of micro-Doppler effect may contaminate ISAR image of the main body and bring great difficulties to the image interpretation[10,11]. The well-known and frequently-used approaches in the extraction and separation of the micro-Doppler are the high-resolution time-frequency analysis techniques[7,12,13]. A four parameters adaptive Chirplet signal representation method has been used for the separation of rotating parts from the target body in Ref. [14]. The empirical-mode decomposition is utilized to estimate accurate parameters of the rotating parts and focus the image of the main body in Ref. [15]. Furthermore, related literature has revealed the application of the micro-Doppler effect in automatic target recognition, the urban sensing and indoor sensing, the gait and activity analyses of pedestrians and *etc.*[12,14,16−21]. The image processing algorithms have also been introduced for the separation of the micro-Doppler features, such as the Radon transform[22] and the Hough Transform (HT)[10,23]. In Ref. [10], an extended Hough transform is put forward to extract micro-Doppler feature by detecting the straight lines and the sinusoids on the spectrogram. This method is mainly based on two advantages of Hough transform, including the ability to detect sinusoids and the stability and robustness when working on images where noise is present. The micro-Doppler effect in Bi-ISAR system as well as in Multi-static imaging radar system has also been considered in Refs. [24,25]. Although the resolution and micro-Doppler effect in Bi-ISAR system of the moving targets is briefly discussed in Ref. [24], more detailed analysis and micro-Doppler feature extraction algorithms are necessary to be researched, which motivates this paper.

In this study, we first introduce the Bi-ISAR geometry and then discuss some basic issues in Section 2, including the imaging supporting region partition in two-dimensional Bi-static plane, the range resolution and the azimuth resolution. Particularly, for avoiding the calculation of the viewing angle diversity of the target, we introduce a definition called con-Doppler bandwidth, which is used to analyze the azimuth resolution and its spatial-variety characteristic. Then the three-dimensional micro-Doppler effect induced by the vibration and the rotation of targets in Bi-static system are investigated in Section 3. Section 4 is devoted to the discussion of the extraction of the micro-motion information. There, two terms, namely the spatial influence factor of Bi-ISAR and the additional phase term, are introduced to describe the diversity of the micro-motion information between the Bi-ISAR system and the Mono-ISAR system. For extracting the real micro-motion information, the extended Hough transform is modified to eliminate the influence of the spatial influence factor of Bi-ISAR and the additional phase term. Finally, some simulations and imaging results are presented in Section 5.

2 Bi-ISAR Model and Resolution Analysis

Similar to the conventional ISAR system, the range resolution and the azimuth resolution in Bi-ISAR system are obtained via transmitting wide bandwidth pulses and using Doppler frequency shift induced by the relative motion of the target with respect to the radar, respectively. Nevertheless, the two-dimensional resolutions in Bi-ISAR system are provided with the characteristic of the spatial-dependent, that is, the two-dimensional resolutions of the target vary with its location in Bi-ISAR system. Hence, the two-dimensional resolutions in Bi-ISAR system are more complex than that of in the Mono-ISAR system. In this section, the imaging supporting region partition is

first investigated before we discuss the two-dimensional resolutions.

2.1 Supporting regions partition

A two-dimensional coordinate system is shown in Fig. 1, also called the Bi-static plane[26]. The distance L between the transmitter and the receiver is called *baseline* simply; R_{TP} is the distance of the target to the transmitter; R_{RP} is the distance of the target to the receiver; β is the *Bi-static angle* between the transmitter-target line and the receiver-target line. The arcs are the *isolines* of Bi-static angle. The blank Area 1 is defined as Bi-ISAR imaging supporting region, the light shading Area 2 is defined as the Quasi-Mono-ISAR imaging supporting region, and the dark shadow Area 3 is defined as the SISAR imaging supporting region.

The acquirement of Bi-ISAR images is based on the back-scattering characteristics of moving targets and the Bi-static configurations with separated transmitter and receiver. The region difference of Electromagnetic scattering (Back-scattering or Forward-scattering) characteristics appears rather obvious in Bi-static plane. Not all locations in Bi-static radar plane are suitable for imaging by using Bi-ISAR system. Thus it is necessary to consider the imaging supporting regions partition in Bi-static plane firstly.

The operation mode of Bi-ISAR system depends on its coverage region and the scattering characteristics of target. Different from the operating regions partition in Ref. [26], we partition the Bi-static radar plane into three operating regions as shown in Fig. 1 taking account of the coverage region and the imaging mode of the Bi-ISAR system.

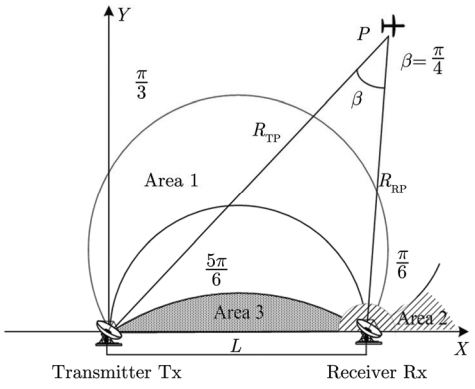

Fig. 1 Imaging area partition

(1) Bi-ISAR imaging supporting region($\pi/6 \le \beta \le 5\pi/6, R_{\mathrm{TP}} \approx R_{\mathrm{RP}}$)

The blank Area 1 in Fig. 1 is defined as the Bi-ISAR imaging supporting region, which can also be called as the co-site region. In this region, the Bi-static effect is obvious and the variety of Bi-static angle within the imaging time is very small. Moreover, the partition of range cell is more stable and the probability of Migration through Resolution Cell (MTRC) occurring is lower in this region. Thus, it becomes major operating area of Bi-ISAR system.

(2) Quasi-Mono-ISAR imaging supporting region $(\beta < \pi/6$ or $R_{\mathrm{RP}} < L/2)$

The light shading Area 2 can be defined as the Quasi-Mono-ISAR imaging supporting region. In this region, the precision of the measurement and the resolution are relatively higher, whereas the ability anti-interference is weak. Furthermore, the Bi-static radar RCS of target is close to the monostatic RCS in this region. Thus, it's suitable for the monostatic imaging radar that identifies targets.

(3) Shadow Inverse Synthetic Aperture Radar (SISAR[27]) imaging supporting region $(\beta > 5\pi/6)$

The dark shadow Area 3 is defined as the SISAR imaging supporting region, which can also be called as the forward-scattering region of Bi-static radar. In this region, the SISAR images of targets can be obtained by using the shadow or the forward-scattering radiolocation method[27]. Based on the Babinet's principle[26], the forward scatter RCS is independent of the wave-absorbing material coated. Thus, in this region, SISAR system has unique advantage of detecting the stealth target[28].

2.2 Bi-ISAR range resolution

As we all know, the range resolution $\rho_{\text{r-Mono-ISAR}}$ in Mono-ISAR system is:

$$\rho_{\text{r-Mono-ISAR}} = \mathrm{c}/(2B) \tag{1}$$

where B is the bandwidth of the transmitted signal and c is the speed of light in free space. It is completely unrelated to the system geometry. The isorange contours in monostatic radar system are a

serial of concentric circles, whose center is radar and difference in range direction is range resolution. The width of the range bin in Mono-ISAR is the space between the two concentric isorange contours. Nevertheless, in Bi-ISAR system, the delay time τ of echoed signal from the target is expressed by

$$\tau = \left(R_{\mathrm{TP}} + R_{\mathrm{RP}}\right)/\mathrm{c} \tag{2}$$

That means, the echoed signal in Bi-ISAR is a function of the range sum $R_{\mathrm{TP}} + R_{\mathrm{RP}}$, where R_{TP} and R_{RP} are the distance of target to transmitter and receiver, respectively. Then the isorange contours in Bi-static radar system are serial of ellipses, whose two foci are the transmitter and receiver sites. Due to the Bi-static angle bisector is perpendicular to the tangent line at the intersection point of the ellipse and the Bi-static angle bisector, the range resolution in Bi-ISAR system is usually defined as the range resolution in the Bi-static angle bisector. Fig. 2 is drawn to convey the basic meaning of the range resolution in Bi-ISAR system for clarity: The two curves are the isoranges whose intersection points with the Bi-static angle bisector are the location of Target 1 and Target 2, and the space between the two intersection points of the Bi-static angle bisector and the adjacent two ellipses is just the range bin of Bi-ISAR system, which is equivalent to the range resolution. Due to the bandwidth of system is B, the difference of range sum, ΔR_B, can be expressed approximately by

$$\Delta R_B \approx \mathrm{c}\Big/\left(2B\cos\left(\frac{\beta}{2}\right)\right) \tag{3}$$

where β is the Bi-static angle. According the define of range resolution of Bi-ISAR, the range resolution in Bi-ISAR $\rho_{\text{r-Bi-ISAR}}$ is ΔR_B.

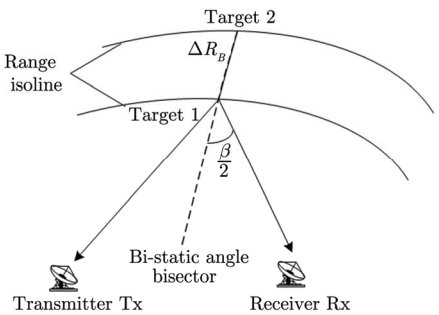

Fig. 2 Bi-ISAR range resolution analysis

Therefore, from the analysis above it can be seen that the range bins are partitioned according to those ellipses, and the range resolution is related with not only the bandwidth but also the position of target, that is, the range resolution in Bi-ISAR system is inversely proportional to the cosine of half of Bi-static angle. It is also the reflection of the space-variant characteristic of the range resolution in Bi-ISAR. In particular, if $\beta = 0$, the expression in Eq. (3) will convert into Eq. (1), that means, the Mono-ISAR system can be regarded as a special example of the Bi-ISAR system.

2.3 Bi-ISAR azimuth resolution

The Doppler bandwidth of the echoed signal can be utilized to express the azimuth resolution in SAR system, *i.e.*,

$$\rho_{\text{a-SAR}} = V / \Delta f_{\mathrm{d}} \tag{4}$$

where V is the velocity of platform and Δf_{d} is the Doppler bandwidth.

We induce a definition called *con-Doppler bandwidth* to express the azimuth resolution in Bi-ISAR system, which helps overcome the difficulty of the targets' viewing angle diversity calculation. As shown in Fig. 3, the point i (here i can be utilized to denote any scatterer point in Fig. 3) moves in Bi-static plane with the velocity V and the included angle between the target's moving direction and the horizontal direction is θ_V. The viewing angles of the transmitter and the receiver at the initial time are α_{T} and α_{R}, respectively. β is the Bi-static angle at the initial time and $\beta + \alpha_{\mathrm{R}} + \alpha_{\mathrm{T}} = \pi$. Then the range sum $R_{\mathrm{T}} + R_{\mathrm{R}}$ at time t_{m} can be rewritten as

$$R_i\left(t_{\mathrm{m}}\right) = R_{\mathrm{Ti}}\left(t_{\mathrm{m}}\right) + R_{\mathrm{Ri}}\left(t_{\mathrm{m}}\right) \tag{5}$$

where

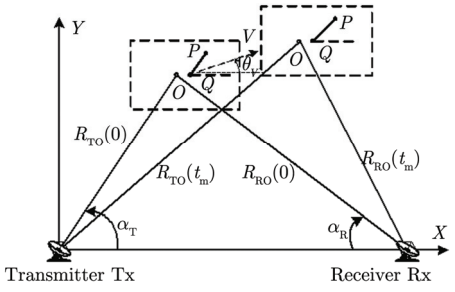

Fig. 3 Bi-ISAR geometry

$$R_{\mathrm{Ti}}(t_{\mathrm{m}})=\sqrt{R_{\mathrm{Ti}}^2(0)+(Vt_{\mathrm{m}})^2+2R_{\mathrm{Ti}}(0)Vt_{\mathrm{m}}\cos(\theta_V-\alpha_{\mathrm{T}})} \tag{6a}$$

$$R_{\mathrm{Ri}}(t_m)=\sqrt{R_{\mathrm{Ri}}^2(0)+(Vt_{\mathrm{m}})^2-2R_{\mathrm{Ri}}(0)Vt_{\mathrm{m}}\cos(\theta_V+\alpha_{\mathrm{R}})} \tag{6b}$$

R_{Ti} and R_{Ri} express the distance of point i to the transmitter and receiver, respectively. Expanding the distances $R_{\mathrm{Ti}}(t_{\mathrm{m}})$ and $R_{\mathrm{Ri}}(t_{\mathrm{m}})$ in Taylor's series and neglecting the higher order terms, the $R_i(t_{\mathrm{m}})$ can be rewritten as

$$\begin{aligned}R_i(t_{\mathrm{m}})&=R_{\mathrm{Ti}}(t_{\mathrm{m}})+R_{\mathrm{Ri}}(t_{\mathrm{m}})\\&\approx R_i(0)+\cos(\theta_V-\alpha_{\mathrm{T}})Vt_{\mathrm{m}}-\cos(\theta_V+\alpha_{\mathrm{R}})Vt_m\\&\quad+\frac{\sin^2(\theta_V-\alpha_{\mathrm{T}})}{2R_{\mathrm{Ti}}(0)}(Vt_{\mathrm{m}})^2+\frac{\sin^2(\theta_V+\alpha_{\mathrm{R}})}{2R_{\mathrm{Ri}}(0)}(Vt_{\mathrm{m}})^2\end{aligned} \tag{7}$$

Assume the transmitted signal is the single frequency signal whose carrier frequency is f_{c}. Then the received signal from the point i can be written as

$$s_i(t,t_{\mathrm{m}})=\exp\left(j2\pi f_{\mathrm{c}}\frac{R_i(t_{\mathrm{m}})}{\mathrm{c}}\right)=\exp\left(j\Phi_i(t_{\mathrm{m}})\right) \tag{8}$$

The con-Doppler frequency can be obtained via the time derivative of the phase term of Eq. (7), *i.e.*,

$$\begin{aligned}f_{\mathrm{d}}&=\frac{1}{2\pi}\frac{\mathrm{d}}{\mathrm{d}t_{\mathrm{m}}}\Phi_i(t_{\mathrm{m}})=\frac{1}{\lambda_{\mathrm{c}}}\frac{\mathrm{d}\left(R_i(t_{\mathrm{m}})\right)}{\mathrm{d}t_{\mathrm{m}}}\\&=\frac{1}{\lambda_{\mathrm{c}}}\left(\left(\cos(\theta_V-\alpha_{\mathrm{T}})-\cos(\theta_V+\alpha_{\mathrm{R}})\right)V\right.\\&\quad\left.+\left(\frac{\sin^2(\theta_V-\alpha_{\mathrm{T}})}{R_{\mathrm{Ti}}(0)}+\frac{\sin^2(\theta_V+\alpha_{\mathrm{R}})}{R_{\mathrm{Ri}}(0)}\right)V^2t_{\mathrm{m}}\right)\end{aligned} \tag{9}$$

From Eq. (9), the Doppler frequency rate can be denoted as

$$\gamma_{\mathrm{a}}=\frac{1}{\lambda_{\mathrm{c}}}V^2\left(\frac{\sin^2(\theta_V-\alpha_{\mathrm{T}})}{R_{\mathrm{Ti}}(0)}+\frac{\sin^2(\theta_V+\alpha_{\mathrm{R}})}{R_{\mathrm{Ri}}(0)}\right) \tag{10}$$

So the con-Doppler bandwidth is given by

$$\Delta f_{\mathrm{d}}=|\gamma_{\mathrm{a}}|T_{\mathrm{a}} \tag{11}$$

where T_{a} stands for the coherent processing time. So, as mentioned previously, the Bi-ISAR azimuth resolution can be expressed as

$$\begin{aligned}\rho_{\text{a-Bi-ISAR}}&=\frac{V}{|\Delta f_{\mathrm{d}}|}=\frac{V}{|\gamma_{\mathrm{a}}|T_{\mathrm{a}}}=\frac{\lambda_{\mathrm{c}}}{VT_{\mathrm{a}}}\\&\quad\cdot\frac{R_{\mathrm{Ti}}(0)R_{\mathrm{Ri}}(0)}{R_{\mathrm{Ri}}(0)\sin^2(\theta_V-\alpha_{\mathrm{T}})+R_{\mathrm{Ti}}(0)\sin^2(\theta_V+\alpha_{\mathrm{R}})}\end{aligned} \tag{12}$$

(1) when $\alpha_{\mathrm{T}}=\pi-\alpha_{\mathrm{R}}$, the Bi-ISAR system converts to the Quasi-Mono-ISAR system. If we consider a special case: $R_{\mathrm{Ti}}(0)=R_{\mathrm{Ri}}(0)$, then the azimuth resolution is

$$\rho_{\text{a-Bi-ISAR}}=\frac{\lambda_{\mathrm{c}}R_{\mathrm{Ti}}(0)}{2VT_{\mathrm{a}}\sin^2(\theta_V-\alpha_{\mathrm{T}})} \tag{13}$$

(2) when $\alpha_{\mathrm{T}}=\alpha_{\mathrm{R}}\neq\pi/2$, and $\beta\neq0$ that also means, $R_{\mathrm{Ti}}(0)=R_{\mathrm{Ri}}(0)$, then the azimuth resolution is given by

$$\rho_{\text{a-Bi-ISAR}}=\frac{\lambda_{\mathrm{c}}R_{\mathrm{Ti}}(0)}{VT_{\mathrm{a}}}\cdot\frac{1}{\sin^2(\theta_V-\alpha_{\mathrm{T}})+\sin^2(\theta_V+\alpha_{\mathrm{T}})} \tag{14}$$

It can be seen from Eq. (14) that the azimuth resolution is directly proportional to the distance of target to transmitter/receiver. In particular, while $\alpha_{\mathrm{T}}=\pi/4,\alpha_{\mathrm{R}}=\pi/4,$ and $\beta=\pi/2$, we have $\theta_V-\alpha_{\mathrm{T}}=-\pi/2+\theta_V+\alpha_{\mathrm{R}}$, which, when substituted in Eq. (14), leads to the following constant azimuth resolution

$$\rho_{\text{a-Bi-ISAR}}=\frac{\lambda_{\mathrm{c}}R_{\mathrm{Ti}}(0)}{VT_{\mathrm{a}}} \tag{15}$$

In the following we consider the characteristic of the spatial-dependent of the azimuth resolution, that is, the influence of the spatial location of target in Bi-ISAR system on the azimuth resolution. It is known from the spatial relationship of Bi-ISAR system that the relationship between target and the system can be determined if any three of parameters R_{Ti}, R_{Ri}, α_{T}, α_{R} are given. And, according to basic trigonometric rules, we have

$$R_{\mathrm{Ri}}(0)=\frac{R_{\mathrm{Ti}}(0)\sin\alpha_{\mathrm{T}}}{\sin\alpha_{\mathrm{R}}} \tag{16}$$

Substituting Eq. (16) and $\alpha_{\mathrm{R}}=\pi-(\alpha_{\mathrm{T}}+\beta)$ into Eq. (14), we also have

$$\begin{aligned}\rho_{\text{a-Bi-ISAR}}&=\frac{\lambda_{\mathrm{c}}R_{\mathrm{Ti}}(0)}{VT_{\mathrm{a}}}\\&\quad\cdot\frac{\sin\alpha_{\mathrm{T}}}{\sin^2(\theta_V-\alpha_{\mathrm{T}})\sin\alpha_{\mathrm{T}}+\sin^2(\theta_V-\alpha_{\mathrm{T}}-\beta)\sin(\alpha_{\mathrm{T}}+\beta)}\end{aligned} \tag{17}$$

Because we mainly focus on the influence of the Bi-static angle on the azimuth resolution, the velocity of target, V, and the initial viewing angles α_{T}, can be viewed as two constants in the following

discussion and, furthermore, the viewing angle α_{T} is limited to the region $(0,\pi/2)$. Carrying out the differentiation with respect to the Bi-static angle β, we have

$$\frac{\mathrm{d}\rho_{\text{a-Bi-ISAR}}}{\mathrm{d}\beta}=-\frac{\lambda_{\mathrm{c}}R_{\mathrm{Ti}}(0)}{VT_{\mathrm{a}}}\frac{\left(-\sin\left(2\left(\theta_V-\alpha_{\mathrm{T}}-\beta\right)\right)\sin\left(\alpha_{\mathrm{T}}+\beta\right)+\sin^2\left(\theta_V-\alpha_{\mathrm{T}}-\beta\right)\cos\left(\alpha_{\mathrm{T}}+\beta\right)\right)\sin\alpha_{\mathrm{T}}}{\left(\sin^2\left(\theta_V-\alpha_{\mathrm{T}}\right)\sin\alpha_{\mathrm{T}}+\sin^2\left(\theta_V-\alpha_{\mathrm{T}}-\beta\right)\sin\left(\alpha_{\mathrm{T}}+\beta\right)\right)^2} \tag{18}$$

While $\theta_V-\alpha_{\mathrm{T}}-\beta=\pm n\pi\ (n=0,1,2,\cdots)$, we have the differentiation $\mathrm{d}\rho_{\text{a-Bi-ISAR}}/\mathrm{d}\beta=0$, then the azimuth resolution will achieve its extremums. In view of the movement direction of target belong in the region $[0,2\pi]$ and $0<\alpha_{\mathrm{T}}+\beta<\pi$, it can be seen that, only if $\theta_V-\alpha_{\mathrm{T}}-\beta$ is 0 or π, the azimuth resolution will achieve its extremum. That means, the maximum value of the azimuth resolution is given by

$$\rho_{\text{a-Bi-ISAR}}=\frac{\lambda_c R_{\mathrm{Ti}}(0)}{VT_{\mathrm{a}}}\frac{1}{\sin^2\left(\theta_V-\alpha_{\mathrm{T}}\right)} \tag{19}$$

From the analysis above we can therefore conclude that the azimuth resolution in Bi-ISAR system is very complex because of the special spatial configuration of Bi-ISAR system. The key factors influencing the azimuth resolution include the movement direction of target, the Bi-static angle, the distance of target to sits, *etc.*. The azimuth resolution is provided with the time-variety characteristic as well as the spatial-variety characteristic.

3 Micro-Doppler Effect Analysis

The micro-Doppler effect is caused by vibration or rotation of a target, or structures on the target and it will induce additional frequency modulations on the received radar signal, which generates side-bands about the target's Doppler frequency [17,29,30]. It can be regarded as a unique signature of an object with movements and provides additional information for the classification, recognition, and identification of the object. This section is devoted to the discussion of the micro-Doppler effect in Bi-ISAR system.

3.1 Micro-Doppler of three-dimensional vibration

As shown in Fig. 4, the transmitter is located at the origin of the radar coordinate system (X,Y,Z) and the receiver is located on the X-axis. The baseline is L and then the coordinate of receiver is $(L,0,0)$. A vibrating target is described in the local coordinate system (x,y,z) whose origin is located at the geometric center of the target. The translational velocity of the target is V. In the radar coordinates (X,Y,Z), we assume that at the initial time the elevation and azimuth angle of the target with respect to transmitter are α_{T} and β_{T}, respectively, and the coordinate of the micro-motion center Point Q of the target at the initial time can be written as $\left(R_{\mathrm{TQ}}(0)\cos\alpha_{\mathrm{T}}\cos\beta_{\mathrm{T}},\ R_{\mathrm{TQ}}(0)\sin\alpha_{\mathrm{T}},\ R_{\mathrm{TQ}}(0)\cos\alpha_{\mathrm{T}}\sin\beta_{\mathrm{T}}\right)$, where $R_{\mathrm{TQ}}(0)$ stands for the distance of the transmitter to the micro-motion center Point Q at the initial time as shown in Fig. 4.

Suppose a scatterer Point P is vibrating at a vibration rate ω with maximum amplitude r, and, at the initial time, the elevation and azimuth angle of the scatterer point in the local coordinates system (x,y,z) is α_P,β_P, respectively. Then the coordinate of the scatterer point in the local coordinates system at time t_{m} is $\left(D_{t_{\mathrm{m}}}\cos\alpha_P\cdot\cos\beta_P, D_{t_{\mathrm{m}}}\sin\alpha_P, D_{t_{\mathrm{m}}}\cos\alpha_P\sin\beta_P\right)$, where $D_{t_{\mathrm{m}}}$ stands for the distance of the scatterer point to the micro-motion center of target at the time t_{m}. It can be expressed as follows[30]

$$D_{t_{\mathrm{m}}}=r\sin\left(\omega t_{\mathrm{m}}+\theta\right) \tag{20}$$

where θ is the vibrating phase of the scatterer point at the initial time. So in the local coordinate system (x,y,z), the vector from the micro-motion center Point Q to the scatterer Point P is

$$\mathbf{QP}(t_{\mathrm{m}})=\left[D_{t_{\mathrm{m}}}\cos\alpha_P\cos\beta_P\quad D_{t_{\mathrm{m}}}\sin\alpha_P\quad D_{t_{\mathrm{m}}}\cos\alpha_P\sin\beta_P\right]^{\mathrm{T}} \tag{21}$$

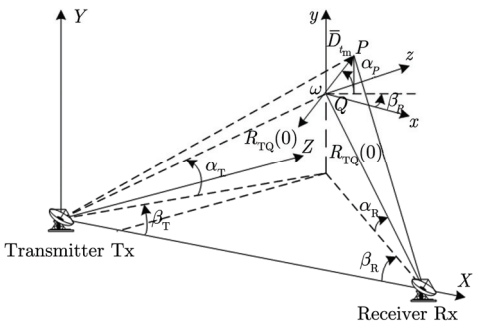

Fig. 4 Model of three-dimensional vibration target

From Fig. 4, in the radar coordinates (X,Y,Z), the vector from the transmitter and the receiver to the scatterer Point P can be expressed as

$$\mathbf{TP}(t_{\mathrm{m}})=\mathbf{TQ}(t_{\mathrm{m}})+\mathbf{QP}(t_{\mathrm{m}})=\mathbf{TQ}(0)+\boldsymbol{V}t_{\mathrm{m}}+\mathbf{QP}(t_{\mathrm{m}}) \tag{22a}$$

$$\mathbf{RP}(t_{\mathrm{m}})=\mathbf{RQ}(t_{\mathrm{m}})+\mathbf{QP}(t_{\mathrm{m}})=\mathbf{RQ}(0)+\boldsymbol{V}t_{\mathrm{m}}+\mathbf{QP}(t_{\mathrm{m}}) \tag{22b}$$

respectively, where $\mathbf{TQ}(t_{\mathrm{m}})$, $\mathbf{RQ}(t_{\mathrm{m}})$ express the vector from the transmitter and the receiver to the micro-motion center Point Q in the radar coordinates (X,Y,Z), respectively. So the range sum of the scatterer Point P at time t_{m} can be denoted as

$$R_P(t_{\mathrm{m}})=\left\|\mathbf{TP}(t_{\mathrm{m}})\right\|+\left\|\mathbf{RP}(t_{\mathrm{m}})\right\| \tag{23}$$

where $\|\cdot\|$ stands for the Euclidean norm. Similar to Eq. (9), the micro-Doppler frequency induced by the vibration of the scatterer point is

$$\begin{aligned}f_{\mathrm{D}}&=\frac{1}{2\pi}\frac{\mathrm{d}\Phi_P(t_{\mathrm{m}})}{\mathrm{d}t_{\mathrm{m}}}=\frac{1}{\lambda_{\mathrm{c}}}\frac{\mathrm{d}}{\mathrm{d}t_{\mathrm{m}}}R_P(t_{\mathrm{m}})\\&=\frac{1}{\lambda_{\mathrm{c}}\left\|\mathbf{TP}(t_{\mathrm{m}})\right\|}\frac{\mathrm{d}}{\mathrm{d}t_{\mathrm{m}}}\left\{\left(\mathbf{TP}(t_{\mathrm{m}})\right)^{\mathrm{T}}\times\left(\mathbf{TP}(t_{\mathrm{m}})\right)\right\}\\&\quad+\frac{1}{\lambda_{\mathrm{c}}\left\|\mathbf{RP}(t_{\mathrm{m}})\right\|}\frac{\mathrm{d}}{\mathrm{d}t_{\mathrm{m}}}\left\{\left(\mathbf{RP}(t_{\mathrm{m}})\right)^{\mathrm{T}}\times\left(\mathbf{RP}(t_{\mathrm{m}})\right)\right\}\\&=\frac{1}{\lambda_{\mathrm{c}}}\frac{\mathrm{d}}{\mathrm{d}t_{\mathrm{m}}}\left\{\left(\mathbf{TP}(t_{\mathrm{m}})\right)^{\mathrm{T}}\right\}\boldsymbol{n}_{\mathrm{T}}+\frac{1}{\lambda_{\mathrm{c}}}\frac{\mathrm{d}}{\mathrm{d}t_{\mathrm{m}}}\left\{\left(\mathbf{RP}(t_{\mathrm{m}})\right)^{\mathrm{T}}\right\}\boldsymbol{n}_{\mathrm{R}}\\&=\frac{1}{\lambda_{\mathrm{c}}}\left(\boldsymbol{V}+\frac{\mathrm{d}}{\mathrm{d}t_{\mathrm{m}}}\left(\mathbf{QP}(t_{\mathrm{m}})\right)\right)^{\mathrm{T}}\left(\boldsymbol{n}_{\mathrm{T}}+\boldsymbol{n}_{\mathrm{R}}\right)\\&=\frac{1}{\lambda_{\mathrm{c}}}\left(\boldsymbol{V}+\frac{\mathrm{d}}{\mathrm{d}t_{\mathrm{m}}}\left(\mathbf{QP}(t_{\mathrm{m}})\right)\right)^{\mathrm{T}}\boldsymbol{n}_P\end{aligned} \tag{24}$$

where

$$\boldsymbol{n}_{\mathrm{T}}=\frac{\mathbf{TP}(t_{\mathrm{m}})}{\left\|\mathbf{TP}(t_{\mathrm{m}})\right\|},\boldsymbol{n}_{\mathrm{R}}=\frac{\mathbf{RP}(t_{\mathrm{m}})}{\left\|\mathbf{RP}(t_{\mathrm{m}})\right\|}$$

and $\boldsymbol{n}_P=\boldsymbol{n}_{\mathrm{T}}+\boldsymbol{n}_{\mathrm{R}}$.

For the convenience of analyzing micro-Doppler effect in Bi-static radar system, we assume the translational velocity $\boldsymbol{V}$ is zero. So the micro-Doppler frequency induced by the vibration of the scatterer point is

$$f_{\text{VirP-micro-Doppler}}=\frac{1}{\lambda_{\mathrm{c}}}\left(\frac{\mathrm{d}}{\mathrm{d}t_{\mathrm{m}}}\left(\mathbf{QP}(t_{\mathrm{m}})\right)\right)^{\mathrm{T}}\boldsymbol{n}_P \tag{25}$$

If the micro-Doppler induced by the target vibration is considered in the two-dimensional Bi-ISAR plane, and the moving direction is parallel with the level direction, then the Eq. (25) can be rewritten as (the detailed derivation is concluded in the Appendix A)

$$f_{\text{VirP-micro-Doppler}}=\frac{1}{\lambda_{\mathrm{c}}}r\omega\cdot\cos(\omega t_{\mathrm{m}}+\theta)\cdot F\cos(\alpha_P-\varphi) \tag{26}$$

where $F=\sqrt{\left(\sin\alpha_{\mathrm{T}}+\sin\alpha_{\mathrm{R}}\right)^2+\left(\cos\alpha_{\mathrm{T}}-\cos\alpha_{\mathrm{R}}\right)^2}$ is defined as *the spatial influence factor* of Bi-ISAR and $\varphi=\arctan\left(\left(\sin\alpha_{\mathrm{T}}+\sin\alpha_{\mathrm{R}}\right)/\left(\cos\alpha_{\mathrm{T}}-\cos\alpha_{\mathrm{R}}\right)\right)$ is *the additional phase term*.

3.2 Micro-Doppler of three-dimensional rotation

The geometry of Bi-Static radar and a target with three-dimensional rotations is depicted in Fig. 5, in which the parameters of the Bi-static radar and the construction of the two coordinate systems, (X,Y,Z) and (x,y,z), are the same to that of in Fig. 4. For the convenience of showing the rotation of target, a reference coordinate system (X',Y',Z') is introduced, which is parallel to the radar coordinate system (X,Y,Z) and located at the origin of the local coordinate system (x,y,z).

Assuming that the target moves with the velocity $\boldsymbol{V}$ in the radar coordinate system and rotates with the angular velocity $\boldsymbol{w}=\begin{bmatrix}w_x & w_y & w_z\end{bmatrix}^{\mathrm{T}}$ in the local coordinate system. The angular velocity can also be represented in the reference coordinate system (X',Y',Z') as $\boldsymbol{w}'=\begin{bmatrix}\omega_{X'} & \omega_{Y'} & \omega_{Z'}\end{bmatrix}$ and we have the following relationship

$$\boldsymbol{w}'=\boldsymbol{R}_{\text{init}}\cdot\boldsymbol{w} \tag{27}$$

where $\boldsymbol{R}_{\text{init}}$ is the initial rotation matrix between the local coordinate system and the reference coordinate system, which is determined by the initial Euler angle (ϕ,ψ,ξ) and can be represented as[29]

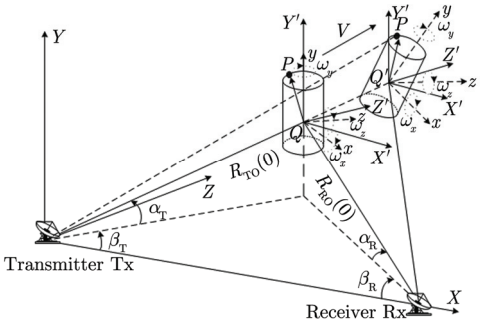

Fig. 5 Model of three-dimensional rotation target

$$\boldsymbol{R}_{\text{init}}=\begin{bmatrix}\cos\phi & -\sin\phi & 0\\ \sin\phi & \cos\phi & 0\\ 0 & 0 & 1\end{bmatrix}\cdot\begin{bmatrix}1 & 0 & 0\\ 0 & \cos\psi & -\sin\psi\\ 0 & \sin\psi & \cos\psi\end{bmatrix}\begin{bmatrix}\cos\xi & -\sin\xi & 0\\ \sin\xi & \cos\xi & 0\\ 0 & 0 & 1\end{bmatrix} \quad (28)$$

By using the initial rotation matrix, a scatterer Point P of the target with the initial location, $\boldsymbol{r}_0=\begin{bmatrix}x_0 & y_0 & z_0\end{bmatrix}^{\mathrm{T}}$, in the local coordinate system can also be rewritten as $\boldsymbol{r}_P(0)=\boldsymbol{R}_{\text{init}}\boldsymbol{r}_0$ in the reference coordinate system. Furthermore, in the reference coordinate system (X',Y',Z'), the vector from the micro-motion center Point Q to the scatterer Point P at time t_{m} is

$$\mathbf{QP}(t_{\text{m}})=\boldsymbol{r}_{P'}(t_{\text{m}})=\boldsymbol{R}_{\text{rot}}(t_{\text{m}})\cdot\boldsymbol{r}_P(0) \quad (29)$$

$$\boldsymbol{R}_{\text{rot}}(t_{\text{m}})=\exp\{\widehat{\boldsymbol{w}}\,t_{\text{m}}\} \quad (30)$$

where $\boldsymbol{R}_{\text{rot}}(t_m)$ is the rotation matrix at time t_{m}, $\widehat{\boldsymbol{w}}$ is the skew-symmetric matrix of $\boldsymbol{w}'$ and is given by[29]

$$\widehat{\boldsymbol{w}}=\begin{bmatrix}0 & -\omega_{Z'} & \omega_{Y'}\\ \omega_{Z'} & 0 & -\omega_{X'}\\ -\omega_{Y'} & \omega_{X'} & 0\end{bmatrix} \quad (31)$$

Then, in the radar coordinate system (X,Y,Z), the respective range vectors of the scatterer Point P to the transmitter and the receiver at time t_{m} can be written as

$$\begin{aligned}\mathbf{TP}(t_{\text{m}})&=\mathbf{TQ}(t_{\text{m}})+\mathbf{QP}(t_{\text{m}})\\&=\mathbf{TQ}(0)+\boldsymbol{V}t_{\text{m}}+\boldsymbol{R}_{\text{rot}}(t_{\text{m}})\cdot\boldsymbol{r}_P(0) \quad (32a)\\ \mathbf{RP}(t_{\text{m}})&=\mathbf{RQ}(t_{\text{m}})+\mathbf{QP}(t_{\text{m}})\\&=\mathbf{RQ}(0)+\boldsymbol{V}t_{\text{m}}+\boldsymbol{R}_{\text{rot}}(t_{\text{m}})\cdot\boldsymbol{r}_P(0) \quad (32b)\end{aligned}$$

respectively, where $\mathbf{TQ}(t_{\text{m}})$ and $\mathbf{RQ}(t_{\text{m}})$ are the same with Eq. (22).

Hence, similar to that of discussion in Subsection 3.1, the Doppler shift induced by the movement of the scatterer point can be expressed as

$$\begin{aligned}f_{\text{D}}&=\frac{1}{2\pi}\frac{\mathrm{d}\Phi_P(t_{\text{m}})}{\mathrm{d}t_{\text{m}}}=\frac{1}{\lambda}\frac{\mathrm{d}}{\mathrm{d}t_{\text{m}}}R_P(t_{\text{m}})\\&=\frac{1}{\lambda}\left[\boldsymbol{V}+\frac{\mathrm{d}}{\mathrm{d}t_{\text{m}}}\left(e^{\widehat{\boldsymbol{w}}\,t_{\text{m}}}\cdot\boldsymbol{r}_P(0)\right)\right]^{\mathrm{T}}\boldsymbol{n}_P\\&=\frac{1}{\lambda}\left[\boldsymbol{V}+\widehat{\boldsymbol{w}}\times\mathbf{QP}(t_{\text{m}})\right]^{\mathrm{T}}\boldsymbol{n}_P \quad (33)\end{aligned}$$

where $\boldsymbol{n}_P$ is the same to Eq. (24).

Similarly, assume the translational velocity $\boldsymbol{V}$ is zero, the micro-Doppler induced by rotation is given by

$$f_{\text{RotP-micro-Doppler}}=\frac{1}{\lambda_{\text{c}}}\left[\widehat{\boldsymbol{w}}\times\mathbf{QP}(t_{\text{m}})\right]^{\mathrm{T}}\boldsymbol{n}_P \quad (34)$$

In the two-dimensional Bi-ISAR plane, and the moving direction is parallel with the level direction, Eq. (34) can be converted to (the detailed derivation is concluded in the Appendix B).

$$f_{\text{RotP-micro-Doppler}}=-\frac{1}{\lambda_{\text{c}}}\omega r\cdot F\sin(\omega t_{\text{m}}+\theta-\varphi) \quad (35)$$

where F and φ are the spatial influence factor of Bi-ISAR and the additional phase term, respectively.

4 Extraction of Micro-Doppler

To make easier to discussion, we utilize Eq. (26) and Eq. (35) throughout this subsection.

As shown in Fig. 3, we assume that $\theta_V=0$ for the sake of simplicity, then the target moves with a velocity V along the horizontal direction, the distance of the receiver to the transmitter is L. The target model is composed of some main body scatterers, such as the target center point $O(x_{\text{ref}},y_{\text{ref}})$ and the micro-motion center point $Q(x_Q,y_Q)$, and some micro-motion scatterer, which includes the vibration scatterers as well as the rotation scatterers.

Assume the transmitted LFM signal is

$$s(t)=\text{rect}\left(\frac{t}{T_P}\right)\exp\left(j2\pi\left(f_{\text{c}}t+\frac{1}{2}kt^2\right)\right) \quad (36)$$

where T_P is pulse width, f_{c} is the carrier frequency and k is the chirp rate.

Ignoring the scattering intensity information, the received signal at time t_{m} from a scatterer Point i is

$$\begin{aligned}s_i(t,t_{\text{m}})=&\,\text{rect}\left(\frac{t-R_i(t_{\text{m}})/\text{c}}{T_P}\right)\\&\cdot\exp\left(j2\pi\left(f_{\text{c}}\left(t-\frac{R_i(t_{\text{m}})}{\text{c}}\right)+\frac{1}{2}k\left(t-\frac{R_i(t_{\text{m}})}{\text{c}}\right)^2\right)\right)\end{aligned} \quad (37)$$

If the scatterer point i stands for the micro-motion Point P, then the instantaneous sum

rang, $R_P(t_{\mathrm{m}})$, can be expressed as (the detailed derivation can be found in the Appendix A and Appendix B)

$$R_P(t_{\mathrm{m}}) = R_Q(0) + L\cdot Vt_{\mathrm{m}} + r\sin(\omega t_{\mathrm{m}}+\theta) \cdot\left(\cos(\alpha_P-\alpha_{\mathrm{T}})-\cos(\alpha_P+\alpha_{\mathrm{R}})\right) \quad (38)$$

where the scatterer P denote the vibration scatterer and $L{=}\cos\alpha_{\mathrm{T}}-\cos\alpha_{\mathrm{R}}$.

$$R_P(t_{\mathrm{m}}) = R_Q(0) + L\cdot Vt_{\mathrm{m}} + r\left(\cos(\omega t_{\mathrm{m}}+\theta-\alpha_{\mathrm{T}})-\cos(\omega t_{\mathrm{m}}+\theta+\alpha_{\mathrm{R}})\right) \quad (39)$$

where the scatterer P denote the rotation scatterer.

Taking the received signal of target center O as the reference signal, $s_{\mathrm{ref}}(t,t_{\mathrm{m}})$, then we have

$$s_{\mathrm{ref}}(t,t_{\mathrm{m}}) = \mathrm{rect}\left(\frac{t-R_{\mathrm{ref}}(t_{\mathrm{m}})/c}{T_{\mathrm{ref}}}\right) \cdot\exp\left(j2\pi\left(f_{\mathrm{c}}\left(t-\frac{R_{\mathrm{ref}}(t_{\mathrm{m}})}{\mathrm{c}}\right)+\frac{1}{2}k\left(t-\frac{R_{\mathrm{ref}}(t_{\mathrm{m}})}{\mathrm{c}}\right)^2\right)\right) \quad (40)$$

where $R_{\mathrm{ref}}(t_{\mathrm{m}})$ expresses the instantaneous sum range of the center Point O at time t_{m}. After dechirp processing, we have

$$\begin{aligned} s_{\mathrm{ci}}(t,t_{\mathrm{m}}) &= s_i(t,t_{\mathrm{m}})\cdot s_{\mathrm{ref}}^*(t,t_{\mathrm{m}}) \\ &= \mathrm{rect}\left(\frac{t-R_i(t_{\mathrm{m}})/\mathrm{c}}{T_{\mathrm{ref}}}\right) \cdot\exp\left(-j\frac{2\rho k}{\mathrm{c}}\left(t-\frac{R_{\mathrm{ref}}(t_{\mathrm{m}})}{\mathrm{c}}\right)\right) \\ &\quad\cdot\exp\left(-j\frac{2\pi}{\lambda_{\mathrm{c}}}\Delta R_i(t_{\mathrm{m}})\right)\cdot\exp\left(j\frac{\pi k}{\mathrm{c}^2}\Delta R_i^2(t_{\mathrm{m}})\right) \end{aligned} \quad (41)$$

where $\Delta R_i(t_{\mathrm{m}}) = R_i(t_{\mathrm{m}}) - R_O(t_{\mathrm{m}})$. The third phase term in Eq. (41) is the Residual Video Phase (RVP) error and it can be compensated easily. Taking Fourier transform of $s_{\mathrm{ci}}(t,t_{\mathrm{m}})$ respect to the fast time t, we obtain the range reconstruction of the target as follows

$$S_{\mathrm{ci}}(f,t_{\mathrm{m}}) = T_P\mathrm{sinc}\left(T_P\left(f+\frac{k}{\mathrm{c}}\Delta R_i(t_{\mathrm{m}})\right)\right) \cdot\exp\left(-j\frac{2\pi}{\lambda_{\mathrm{c}}}\Delta R_i(t_{\mathrm{m}})\right) \quad (42)$$

It can be seen that the value of the range profiles will peak at

$$f_i = -\frac{k}{\mathrm{c}}\Delta R_i(t_{\mathrm{m}}) \quad (43)$$

By multiplying with the coefficient $-\mathrm{c}/k$, the frequency f_i can be translated to provide the distance difference of $\Delta R_i(t_{\mathrm{m}}) = R_i(t_{\mathrm{m}}) - R_O(t_{\mathrm{m}})$. Then we obtain the range distribution of the scatterer relative to the reference point on the Bi-static angle sector. Furthermore, when the scatterer i stands for the micro-motion center Point Q, the vibration scatterer and the rotation scatterer, respectively, we have

$$f_Q = -\frac{k}{\mathrm{c}}\Delta R_Q(t_{\mathrm{m}}) \approx -\frac{k}{\mathrm{c}}\Delta R_Q(0) \quad (44a)$$

$$\begin{aligned} f_{\mathrm{VirP}} &= -\frac{k}{\mathrm{c}}\Delta R_P(t_{\mathrm{m}}) \approx -\frac{k}{\mathrm{c}}\left(\Delta R_Q(t_{\mathrm{m}}) + r\sin(\omega t_{\mathrm{m}}+\theta)\left(\cos(\alpha_P-\alpha_{\mathrm{T}})-\cos(\alpha_P+\alpha_{\mathrm{R}})\right)\right) \\ &= f_Q - \frac{k}{\mathrm{c}}r\cdot\sin(\omega t_{\mathrm{m}}+\theta)\cdot F\cos(\alpha_P-\varphi) \end{aligned} \quad (44b)$$

$$\begin{aligned} f_{\mathrm{RotP}} &= -\frac{k}{\mathrm{c}}\Delta R_P(t_{\mathrm{m}}) \approx -\frac{k}{c}\left(\Delta R_Q(t_{\mathrm{m}}) + r\left(\cos(\omega t_{\mathrm{m}}+\theta-\alpha_{\mathrm{T}})-\cos(\omega t_{\mathrm{m}}+\theta+\alpha_{\mathrm{R}})\right)\right) \\ &= f_Q - \frac{k}{\mathrm{c}}r\cdot F\cos(\omega t_{\mathrm{m}}+\theta-\varphi) \end{aligned} \quad (44c)$$

where $F = \sqrt{(\sin\alpha_{\mathrm{T}}+\sin\alpha_{\mathrm{R}})^2+(\cos\alpha_{\mathrm{T}}-\cos\alpha_{\mathrm{R}})^2}$ and $\varphi = \arctan\left((\sin\alpha_{\mathrm{T}}+\sin\alpha_{\mathrm{R}})/(\cos\alpha_{\mathrm{T}}-\cos\alpha_{\mathrm{R}})\right)$, we named them as *the spatial influence factor* of Bi-ISAR and *the additional phase term*, respectively. It is not hard to find that the position of the micro-motion center Point Q on the frequency axis is immovably and so are the other main body scatterers, and the micro-motion scatterers change with the slow-time t_{m} periodically. Hence, similar to that of in Mono-ISAR system[10], the spectrogram in Bi-ISAR system, which is a 2-D function of frequency (or distance) and slow time, will consist of straight lines induced by main body scatterers and sinusoids induced by micro-motion scatterers. And the sinusoid period is the same with the vibration or rotation period of the scatterer. However, it can also be found from Eq. (44b) and Eq. (44c) that the spatial characteristic of Bi-ISAR system will influence the position of the micro-motion scatterers on the frequency axis as well as the distribution of the micro-motion scatterers on the spectrogram plane accordingly. Hence, the extracted

sinusoid parameters by immediately using the Extended Hough Transform (EHT) described in Ref. [10] cannot represent the real vibration or rotation radii and the real vibration or rotation direction of the micro-motion scatterers. Then the influence of the spatial influence factor of Bi-ISAR and the additional phase term must be eliminated for the rotation or vibration information to be obtained exactly. This is an essential difference between monostatic radar system and Bi-static radar system. Therefore, the spatial relationship between the target and the Bi-static radar must be estimated accurately and the extracted sinusoid parameters by immediately using the extended Hough transform must be transformed to achieve the real micro-motion features. The detailed parameters transform processing will be presented in the following simulation.

5 Simulations and Discussions

In this section, some simulation results are given to verify the theoretical derivation. Firstly the azimuth resolution in Bi-ISAR system is discussed. Secondly, the simulations about Micro-Doppler effect in Bi-ISAR system are conducted and the imaging result of a scatterer point model is presented.

5.1 Azimuth resolution in Bi-ISAR system

Assuming that the wavelength of the transmitted radar signal $\lambda_c = 0.03$ m, the distances of the target's center to the transmitter and the receiver as shown in Fig. 3 are $R_{\mathrm{Ti}}(0) = R_{\mathrm{Ri}}(0) = 100$ km, the velocity of target is $V = 300$ m/s and the coherent integrate time is $T_a = 5$ s. To make sure that the target's location is in the Bi-ISAR imaging supporting region, the viewing angles of the transmitter α_T is limited in $(\pi/6, \pi/3)$. Then we consider the influence of the target's moving direction on the azimuth resolution firstly.

Taking $\alpha_T = \alpha_R$ and the value range of the target's moving direction θ within $[0, 2\pi]$, the distribution of the azimuth resolution can be depicted in Fig. 6. It can be seen that the diversity of the azimuth resolution at the different location is obviously. This diversity is determined by the spatial configuration of Bi-ISAR system and it reflects the spatial-variety characteristic of the azimuth resolution.

In the following we compare the azimuth resolution in Bi-ISAR system with that of in the Mono-ISAR system.

Let the viewing angles of the transmitter $\alpha_T = \pi/6, \pi/4, \pi/3$, respectively, then we can configure three different Bi-ISAR systems. At the same time, a transmitter in Bi-ISAR can also be employed as a receiver so as to a Mono-ISAR can be constructed. The distribution of the azimuth resolution both in Mono-ISAR system and in Bi-ISAR system under the three parameter sets are shown in Fig. 7, where the solid line and the dashed line stand for the azimuth resolution in Bi-ISAR system and in Mono-ISAR system, respectively.

In Fig. 7(a), it can be seen that, when the target's moving direction $\theta = \pi/6, 7\pi/6$, *i.e.*, the target moves along or against radar Line Of Sight (LOS), the azimuth resolution in Mono-ISAR system tend towards infinity. Here, Mono-ISAR system loses its resolution capability in the azimuth direction. The same is true in Fig. 7(b) and Fig. 7(c).

When the target's moving direction θ is limited in $[\pi/2, \pi] \cup [3\pi/2, 2\pi]$, the azimuth resolution in Mono-ISAR system is somewhat better than that of in Bi-ISAR system. However, when θ is limited in $[0, \pi/2] \cup [\pi, 3\pi/2]$, the azimuth resolution in Bi-ISAR system is much better than that of in Mono-ISAR system. It is because the azimuth resolution is influenced by the variation of the tangential velocity of target relative to the Mono-ISAR. In addition, the straight line in

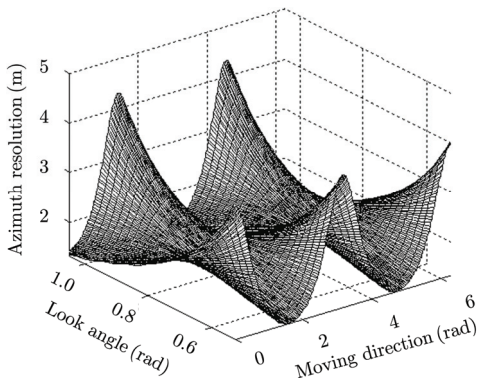

Fig. 6 Azimuth resolution distribution calculated by using Eq. (17)

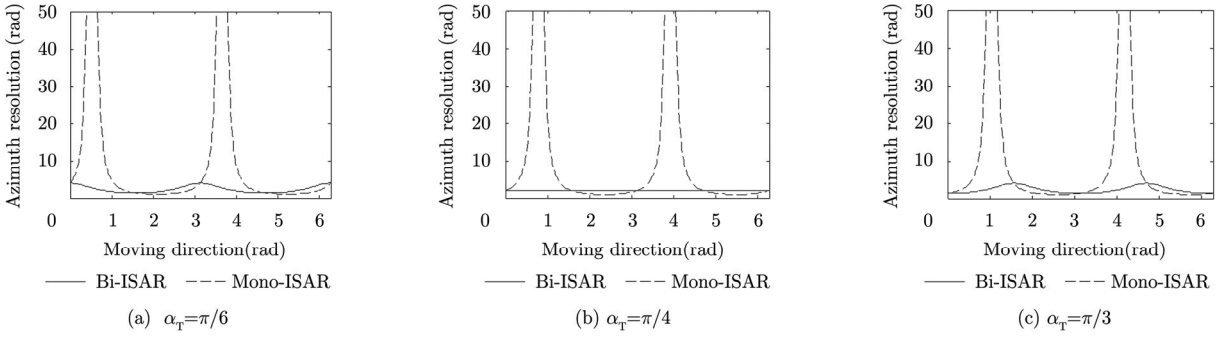

Fig. 7 Azimuth resolution distribution with variation of target moving direction in Bi-ISAR and Mono-ISAR

Fig. 7 (b) shows the azimuth resolution in Bi-ISAR system would not be influenced by the target's moving direction at the moment. It also validates that, when $\alpha_T = \alpha_R = \pi/4$, the azimuth resolution in Bi-ISAR system is constant, which is consistent with the conclusion of Eq. (15).

In a word, the azimuth resolution in Mono-ISAR system is considerable sensitive to the target's moving direction, whereas the azimuth resolution in Bi-ISAR system is not. Even though the variety of the target's moving direction will induce small variation of the azimuth resolution, this influence can be ignored in Bi-ISAR system in comparison with in Mono-ISAR.

In the following we consider the influence of the Bi-static angle on the azimuth resolution.

Let the target's moving direction $\theta = 5\pi/12$, $5\pi/3$, the azimuth resolution in Bi-ISAR system under the three parameter sets, *i.e.*, $\alpha_T = \pi/6, \pi/4, \pi/3$, are depicted in Fig. 8(a) and Fig. 8(b), respectively.

In the case of the target's moving direction $\theta = 5\pi/12$, it can be seen from Fig. 8(a) that, when the Bi-static angle $\beta = \pi/4, \pi/6, \pi/12$, the azimuth resolution is the worst and the relationship mentioned in Section 2 (refer to Eq. (19)), $\theta - \alpha_T - \beta = 0$, is satisfied. In the same way, it can be seen from Fig. 8(b) that, when the Bi-static angle $\beta = \pi/2, 5\pi/12, \pi/3$, the relationship, $\theta - \alpha_T - \beta = \pi$, is also satisfied and the azimuth resolution is the worst. Otherwise, it can be found obviously that the azimuth resolution is influenced by the Bi-static angle β which is determined by the target location in the Bi-static plane.

5.2 Micro-Doppler effect in Bi-ISAR system

In this subsection, four parameter sets of Bi-ISAR system are adopted, whose baseline L are (0,5,10,15) km, respectively, as shown in Fig. 9. While $L = 0$ km, the Bi-ISAR system converts to the Mono-ISAR system. The radar carrier frequency is $f_c = 10$ GHz, the bandwidth is $B = 300$ MHz, and the pulse repetition frequency is PRF = 1000 Hz. Assume that the distance of the target's center to the transmitter is 10km and the target moves parallel with the baseline with velocity V=300 m/s.

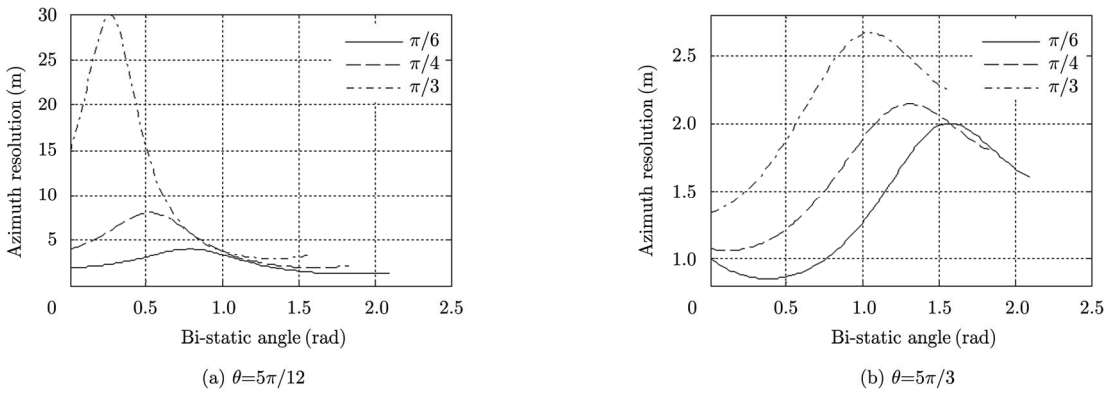

Fig. 8 Azimuth resolution distribution with variation of Bi-satatic angle in Bi-ISAR

The simulation is carried out in the point-scattering mode with five non-rotating scatterers and two rotating scatterers as shown in Fig. 10.

The rotation center's coordinates of two rotating scatterers are $(3,3)$ m and $(0,3)$ m, respectively. Their rotating rates are $(4,12)$ Hz and the rotating radii are $(4,8)$ m, respectively. Both the initial phase is $\theta = 0$.

The spectrograms under the four parameter sets are depicted in Fig. 11, it can be seen that the traces of the non-rotating scattering points are presented as some straight lines that are perpendicular to the frequency axis, and the trace of the rotating scattering points are two sinusoids. Then we can extract the micro-motion information by using the extended Hough transform (In order to clearly focus on the proposed processing method and not get side-tracked by unnecessary discussions, the detailed method about the extended Hough transform can be found in Ref. [10]). However, as mentioned in Section 4, the some extracted information by using the extended Hough transform

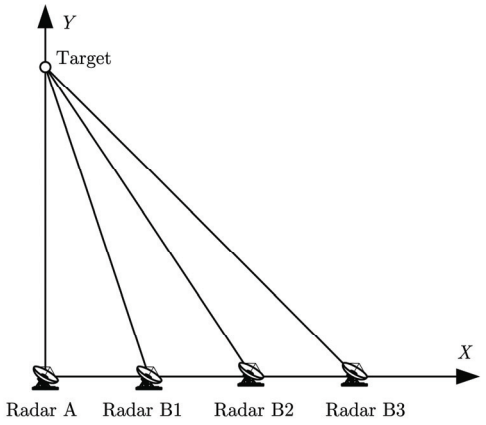

Fig. 9 Bi-ISAR model

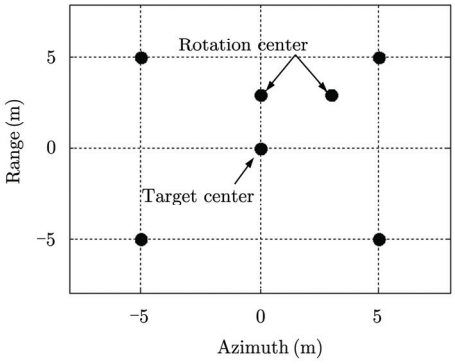

Fig. 10 Scattering point model

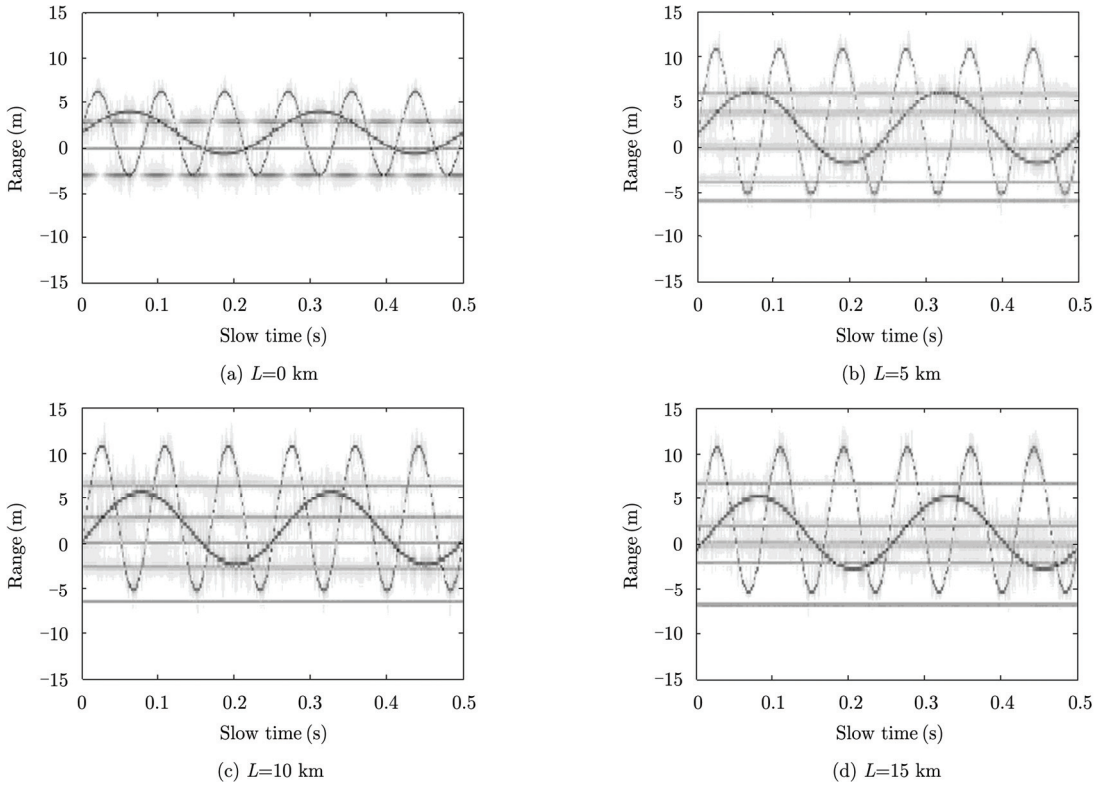

(a) L=0 km (b) L=5 km

(c) L=10 km (d) L=15 km

Fig. 11 Spectrogram of a target that is composed of five nonrotating scattering points and two rotating scattering points

immediately cannot describe the real micro-motion features and the necessary transform processing must be implemented. In fact, according the EHT presented in Ref. [10], the micro-motion features can be obtained directly via the following four-parameter transform

$$f = d \cdot \sin\left(\omega t_{\mathrm{m}} + \varphi_0\right) + l \tag{45}$$

where d is the maximum extent, ω is the angle frequency, $\omega = 2\pi / T_{\mathrm{r}}$, T_{r} is the period, φ_0 is the initial phase, and l can be seen as the baseline and depicts the position of the sinusoid in the frequency axis. Comparing the equation with Eq. (44b) and Eq. (44c), it is not hard to find that the extracted information from the spectrograms Fig. 11, including the rotating radii and the initial phase, are influenced by the spatial influence factor of Bi-ISAR F and the additional phase term φ. For example, from Eq. (44c), the following relationships can be constructed

$$d = r \cdot F \cdot k / \mathrm{c} \tag{46}$$

$$\varphi_0 = \theta - \varphi \tag{47}$$

Hence, the extracted information must be transformed to the real micro-motion features.

The final obtained micro-motion features are presented in Tab. 1. There is a considerable diversity between the extracted features by using the EHT and the real micro-motion features. After the parameters transform processing, the obtained micro-motion features are almost undifferentiated with their real value.

Tab. 1 Micro-motion features under the four parameter sets

Radar parameter		Baseline (km)	F	φ (rad)	Initial phase (rad)		Rotation radius (m)	
					Fore-transform	Aft-transform	Fore-transform	Aft-transform
Mono-ISAR		0			(0, 0)		(4, 8)	
Bi-ISAR	(A, B1)	5	1.95	−1.34	(1.3, 1.3)	(−0.04, −0.04)	(3.9, 7.8)	(4.01, 8.01)
	(A, B2)	10	1.84	−1.18	(1.2, 1.1)	(0.02, −0.08)	(3.7, 7.4)	(4.02, 8.04)
	(A, B3)	15	1.76	−1.08	(1.1, 1.0)	(0.02, −0.08)	(3.5, 7.1)	(3.98, 8.05)

Finally, we give the imaging results of the scattering point model in Fig. 12, where the baseline length in Bi-ISAR was selected as $L = 10$ km. The imaging result before the separation of the micro-Doppler is depicted in Fig. 12(a), it can be seen that the image has been contaminated due to the existence of the micro-Doppler effect. We separate the micro-Doppler from the spectrogram as shown in Fig. 11(c) and the resultant spectrogram is represented in Fig. 12(b). The final imaging result is depicted in Fig. 12(c) and it is as good as what we expect it to be.

6 Conclusions

Because of the special spatial structure of Bi-ISAR, the imaging supporting areas are partitioned according to the different configuration of transmitter and receiver in the paper and then the resolution

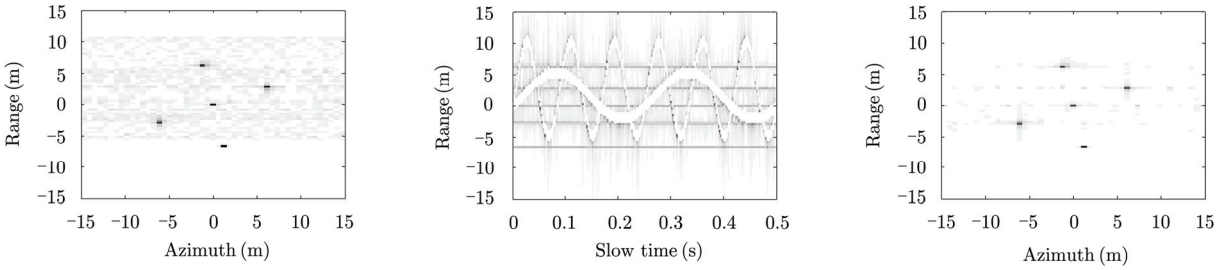

(a) Imaging result before separation of micro-Dopple (b) Spectrogram after separation of micro-Doppler (c) Imaging result after separation of micro-Dopplerr

Fig. 12 Bi-ISAR imaging results of the scattering point model

in Bi-ISAR system, which is quite different from that of in Mono-ISAR system, is analyzed firstly. The three-dimensional micro-Doppler effect induced by the vibration and the rotation of targets is analyzed in detail. It is found that the deduced micro-Doppler effect has obvious Bi-static characteristic. Hence, the extracted micro-motion information by immediately using the extended Hough transform must be transformed with an additional processing to get the real micro-motion features. Some simulation results have been presented to verify the theoretical derivation and the effectiveness of the proposed method. Due to the lack of required real data, we just examine the performance of Bi-ISAR system using simulated data at present. In our future work, we intend to obtain real data of Bi-ISAR and then validate the proposed method.

Appendix A

In this Appendix, we will give the expression of micro-Doppler induced by the target vibration in the two-dimensional Bi-ISAR plane.

Let $\beta_{\mathrm{T}}=\beta_P=\beta_{\mathrm{R}}=0$, the vector from the micro-motion center Point Q to the scatterer Point P in 2-D Bi-static plane at time t_{m} is (refer to Fig. 3)

$$\mathbf{QP}(t_{\mathrm{m}})=\left[D_{t_{\mathrm{m}}}\cos\alpha_P \quad D_{t_{\mathrm{m}}}\sin\alpha_P \quad D_{t_{\mathrm{m}}}\cos\alpha_P\right]^{\mathrm{T}} \tag{A1}$$

And, under the assumption of far-field, we have relationship: $\max\left(D_{t_{\mathrm{m}}}\right)\ll R_{\mathrm{TQ}},R_{\mathrm{RQ}}$; Moreover, we have the following relationship

$$\begin{aligned}\boldsymbol{n}_P&=\boldsymbol{n}_{\mathrm{T}}+\boldsymbol{n}_{\mathrm{R}}\approx\frac{\mathbf{TQ}(0)}{\|\mathbf{TQ}(0)\|}+\frac{\mathbf{RQ}(0)}{\|\mathbf{RQ}(0)\|}\\&=\left[\cos\alpha_{\mathrm{T}}-\cos\alpha_{\mathrm{R}} \quad \sin\alpha_{\mathrm{T}}+\sin\alpha_{\mathrm{R}} \quad 0\right]^{\mathrm{T}}\end{aligned} \tag{A2}$$

Substituting Eq. (A1) and Eq. (A2) in Eq. (25), the micro-Doppler can be rewritten as follow:

$$f_{\text{VirP-micro-Doppler}}=\frac{1}{\lambda_{\mathrm{c}}}r\omega\cdot\cos(\omega t_{\mathrm{m}}+\theta)\cdot F\cos(\alpha_P-\varphi) \tag{A3}$$

where $F=\sqrt{\left(\sin\alpha_{\mathrm{T}}+\sin\alpha_{\mathrm{R}}\right)^2+\left(\cos\alpha_{\mathrm{T}}-\cos\alpha_{\mathrm{R}}\right)^2}$ and $\varphi=\arctan\left(\left(\sin\alpha_{\mathrm{T}}+\sin\alpha_{\mathrm{R}}\right)/\left(\cos\alpha_{\mathrm{T}}-\cos\alpha_{\mathrm{R}}\right)\right)$.

In addition, the range sum of the scatterer Point P to the transmitter and the receiver at time t_{m} can be concluded as follows

$$\begin{aligned}R_P(t_{\mathrm{m}})&=\left\|\mathbf{TP}(t_{\mathrm{m}})\right\|+\left\|\mathbf{RP}(t_{\mathrm{m}})\right\|\\&=\left\|\mathbf{TQ}(t_{\mathrm{m}})\right\|+\mathbf{QP}(t_{\mathrm{m}})^{\mathrm{T}}\cdot\boldsymbol{n}_{\mathrm{T}}\\&\quad+\left\|\mathbf{RQ}(t_{\mathrm{m}})\right\|+\mathbf{QP}(t_{\mathrm{m}})^{\mathrm{T}}\cdot\boldsymbol{n}_{\mathrm{R}}\\&=R_Q(t_{\mathrm{m}})+\mathbf{QP}(t_{\mathrm{m}})^{\mathrm{T}}\cdot\boldsymbol{n}_P\\&=R_Q(t_{\mathrm{m}})+r\sin(\omega t_{\mathrm{m}}+\theta)\\&\quad\cdot\left(\cos(\alpha_P-\alpha_{\mathrm{T}})-\cos(\alpha_P+\alpha_{\mathrm{R}})\right)\end{aligned} \tag{A4}$$

Taking $\theta_V=0$ in Eq. (7) and neglecting the higher order terms, the range sum of a scatterer Point i on target to the transmitter and the receiver can be rewritten as follows

$$R_i(t_{\mathrm{m}})\approx R_i(0)+(\cos\alpha_{\mathrm{T}}-\cos\alpha_{\mathrm{R}})Vt_{\mathrm{m}}=R_i(0)+L\cdot Vt_{\mathrm{m}} \tag{A5}$$

where $L=\cos\alpha_{\mathrm{T}}-\cos\alpha_{\mathrm{R}}$. Let the scatterer point i is the micro-motion center Point Q, we have

$$R_Q(t_{\mathrm{m}})\approx R_Q(0)+L\cdot Vt_{\mathrm{m}} \tag{A6}$$

Substituting Eq. (A6) in Eq. (A4), the range sum of the scatterer Point P to the transmitter and the receiver at time t_m can be rewritten as follows

$$\begin{aligned}R_P(t_{\mathrm{m}})&\approx R_Q(0)+L\cdot Vt_{\mathrm{m}}+r\sin(\omega t_{\mathrm{m}}+\theta)\\&\quad\cdot\left(\cos(\alpha_{\mathrm{T}}-\alpha_P)-\cos(\alpha_{\mathrm{R}}+\alpha_P)\right)\end{aligned} \tag{A7}$$

Appendix B

The coordinate of the scatterer Point P in the local coordinate system (x,y,z) at the initial time can be described as follows

$$\boldsymbol{r}_P(0)=\left[r\cos(\theta) \quad r\sin(\theta) \quad 0\right]^{\mathrm{T}} \tag{A8}$$

And its angular velocity with respect to the local coordinate system (x,y,z) is

$$\boldsymbol{w}=(0,0,w)^{\mathrm{T}} \tag{A9}$$

So the skew-symmetric matrix of $\widehat{\boldsymbol{w}}$ is

$$\widehat{\boldsymbol{w}}=\begin{bmatrix}0&-w&0\\ \omega&0&0\\ 0&0&0\end{bmatrix} \tag{A10}$$

Similar to Eq. (30) in Section 3, the rotation matrix is

$$\begin{aligned}\boldsymbol{R}_{\mathrm{rot}}(t_{\mathrm{m}})&=\exp(\widehat{\boldsymbol{w}}\,t_{\mathrm{m}})\\&=\begin{bmatrix}\cos(wt_{\mathrm{m}})&-\sin(wt_{\mathrm{m}})&0\\ \sin(wt_{\mathrm{m}})&\cos(wt_{\mathrm{m}})&0\\ 0&0&0\end{bmatrix}\end{aligned} \tag{A11}$$

Then the vector from the micro-motion center Point Q to the scatterer Point P is

$$\mathbf{QP}(t_{\mathrm{m}}) = \boldsymbol{R}_{\mathrm{rot}}(t_{\mathrm{m}}) \cdot \boldsymbol{r}_P(0) = \begin{bmatrix} r\cos(wt_{\mathrm{m}} + \theta) \\ r\sin(wt_{\mathrm{m}} + \theta) \\ 0 \end{bmatrix} \quad \text{(A12)}$$

From the above equations and Eq. (34), the micro-Doppler induced by rotation is:

$$\begin{aligned} f_{\text{RotP-micro-Doppler}} &= \frac{1}{\lambda_{\mathrm{c}}}\left[\widehat{\boldsymbol{w}} \times \mathbf{QP}(t_{\mathrm{m}})\right]^{\mathrm{T}} \boldsymbol{n}_P \\ &= \frac{1}{\lambda_{\mathrm{c}}} r\omega\left(\sin(\omega t_{\mathrm{m}} + \theta + \alpha_{\mathrm{R}}) \right. \\ &\quad \left. - \sin(\omega t_{\mathrm{m}} + \theta - \alpha_{\mathrm{T}})\right) \end{aligned} \quad \text{(A13)}$$

where $\boldsymbol{n}_P$ is the same as Eq. (A2). Then the micro-Doppler can be rewritten as follow:

$$f_{\text{RotP-micro-Doppler}} = -\frac{1}{\lambda_{\mathrm{c}}}\omega r \cdot F\sin(\omega t_{\mathrm{m}} + \theta - \varphi) \quad \text{(A14)}$$

and the instantaneous sum rang at time t_{m} can be written as

$$\begin{aligned} R_P(t_{\mathrm{m}}) &= \left\|\mathbf{TP}(t_{\mathrm{m}})\right\| + \left\|\mathbf{RP}(t_{\mathrm{m}})\right\| \\ &= \left\|\mathbf{TQ}(t_{\mathrm{m}})\right\| + \mathbf{QP}^{\mathrm{T}} \cdot \boldsymbol{n}_{\mathrm{T}} + \left\|\mathbf{RQ}(t_{\mathrm{m}})\right\| + \mathbf{QP}^{\mathrm{T}} \cdot \boldsymbol{n}_{\mathrm{R}} \\ &= R_Q(t_{\mathrm{m}}) + \mathbf{QP}^{\mathrm{T}} \cdot \boldsymbol{n}_P \\ &= R_Q(t_{\mathrm{m}}) + \boldsymbol{R}_{\mathrm{rot}}(t_{\mathrm{m}}) \cdot \boldsymbol{r}_P(0) \cdot \boldsymbol{n}_P \\ &= R_Q(t_{\mathrm{m}}) + r\left(\cos(\omega t_{\mathrm{m}} + \theta - \alpha_{\mathrm{T}}) \right. \\ &\quad \left. - \cos(\omega t_{\mathrm{m}} + \theta + \alpha_{\mathrm{R}})\right) \end{aligned} \quad \text{(A15)}$$

Substituting Eq. (A5) in Eq. (A15), it can be rewritten as

$$\begin{aligned} R_P(t_{\mathrm{m}}) \approx R_Q(0) + L \cdot Vt_{\mathrm{m}} + r\left(\cos(\omega t_{\mathrm{m}} + \theta - \alpha_{\mathrm{T}}) \right. \\ \left. - \cos(\omega t_{\mathrm{m}} + \theta + \alpha_{\mathrm{R}})\right) \end{aligned} \quad \text{(A16)}$$

References

[1] Measure N C, Alexander N T, and Taley M T. Unique calibration issues for bistatic radar reflectivity measurements[C]. IEEE National Conference on Radar Systems, Michigan, May 1996: 142–147.

[2] Griffiths H D. From a different perspective: principles, practice and potential of bistatic radar[C]. International Conference on Radar Systems, Australia, Sept. 2003: 1–7.

[3] McAllister C A. Signal processing considerations for an application of bistatic radar[C]. IEEE Region 5th conference on Spanning the Peaks of Electro-technology, Colorado, USA, CO, Mar. 1998: 45–49.

[4] Norland R. Digital signal processing in binary phase coded CW multistatic radar[C]. International Conference on Radar Systems, Australia, Sept. 2003: 99–302.

[5] Palmer J E, Martorella M, and Longstaff I D. Airborne ISAR imaging using the emulated bistatic radar system[C]. European Conference on Synthetic Aperture Radar, Ulm, Germany, May 2004: 375–378.

[6] Burkholder R J, Gupta I J, and Johnoson J T. Comparison of monostatic and bistatic radarimages[J]. *IEEE Antennas and Propagation Magazine*, 2003, 45(3): 41–50.

[7] Lei J and Lu C. Target classification based on micro-Doppler signatures[C]. International Conference on Radar Systems, Arlington, Virginia, May 2005: 179–183.

[8] Chen V C. Spatial and temporal independent component analysis of micro-Doppler features[J]. International Conference on Radar Systems, Arlington, Virginia, May 2005: 348–353.

[9] Sun H X and Liu Z. Micro-Doppler feature extraction for ballistic missile warhead[C]. IEEE International Conference on Information and Automation, Zhangjiajie, China, June 2008: 1334–1336.

[10] Zhang Q, Yeo T S, Tan H S, *et al*.. Imaging of a moving target with rotating parts based on the Hough transform[J]. *IEEE Transactions on Geoscience and Remote Sensing*, 2008, 46(1): 291–299.

[11] Li K M, Luo Y, Chi L, *et al*.. A new separation method for micro-Doppler information of a target with rotating parts[C]. International Conference on Communications, Circuits and Systems, Xiamen, China, May 2008: 1365–1369.

[12] Chen V C. Analysis of radar micro-Doppler signature with time–frequency transform[C]. IEEE Statistical Signal Array Processing, Pocono Manor, PA, Aug. 2000: 463–466.

[13] Thayaparan T, Abrol S, and Riseborough E. Micro-Doppler feature extraction of experimental helicopter data using wavelet and time–frequency analysis[C]. International Conference on Radar Systems, Toulouse, Oct. 2004: 19–22.

[14] Li J and Ling H. Application of adaptive chirplet representation for ISAR feature extraction from targets with rotating parts[J]. *IEE Proceeding-Radar, Sonar and Navigation*, 2003, 150(4): 284–291.

[15] Bai X, Xing M, Zhou F, *et al*.. Imaging of micromotion targets with rotating parts based on empirical-mode decomposition[J]. *IEEE Transactions on Geoscience and Remote Sensing*, 2008, 46(1): 3514–3523.

[16] Chen V C. Micro-Doppler effect of micromotion dynamics: a review[C]. Conference on Independent Component Analysis, Wavelet, and Neural Networks, Orlando, USA, April 2003: 240–249.

[17] Chen V C, Li F, Ho S S, *et al*.. Micro-Doppler effect in radar: phenomenon, model and simulation study[J]. *IEEE Transactions on Aerospace and Electronic Systems*, 2006, 42(1): 2–21.

[18] Thayaparan T, Abrol S, Riseborough E, *et al.*. Analysis of radar micro-Doppler signatures from experimental helicopter and human data[J]. *IEE Proceeding-Radar, Sonar and Navigation*, 2007, 1(4): 289–299.

[19] Ghaleb A, Vignaud L, and Nicolas J M. Micro-Doppler analysis of wheels and pedestrians in ISAR imaging[J]. *IET Signal Processing*, 2008, 2(3): 301–311.

[20] Setlur P, Amin M, and Ahmad F. Urban target classifications using time-frequency micro-Doppler signatures[C]. International Symposium on Signal Processing and Its Applications, sharjah, Feb. 2007: 1–4.

[21] Kim Y and Ling H. Human activity classification based on micro-Doppler signatures using a support vector machine[J]. *IEEE Transactions on Geoscience and Remote Sensing*, 2009, 47(5): 1328–1337.

[22] Stankovic L, Djurovic I, and Thayaparan T. Separation of target rigid body and micro-Doppler effects in ISAR imaging[J]. *IEEE Transactions on Aerospace and Electronic Systems*, 2006, 42(4): 1496–1506.

[23] He S, Zhu Y F, Zhao H Z, *et al.*. Analysis of rotating structures for stepped frequency radar[C]. International Conference on Radar, Adelaide, SA, Sept. 2008: 386–390.

[24] Chen V C, Rosiers A, and Lipps R. Bi-static ISAR range-Doppler imaging and resolution analysis[C]. IEEE Radar Conference, Pasadena CA, May 2009: 1–5.

[25] Liang X J, Zhang Q, Zhu M, *et al.*. Analysis of micro-Doppler effect in SIMO radar[C]. The 2nd International Conference on Signal Processing Systems, Dalian, China, July 2010: 343–346.

[26] Skolnik M I. Radar Handbook[M]. 3rd Ed. New York, USA, McGraw-Hill, 1992.

[27] Chapurskiy V V and Sablin V N. SISAR: shadow inverse synthetic aperture radiolocation[C]. IEEE International Radar Conference, Alexandria Virginia, May 2000: 322–328.

[28] 张涛, 张群, 罗斌凤, 等. 基于时频分析的双基地前向散射雷达侧影成像[J]. 电子学报, 2001, 29(6): 1–4.
Zhang Tao, Zhang Qun, Luo Bin-feng, *et al.*. Shadow imaging for bistatic radar based on forward scattering by joint time frequency analysis[J]. *Acta Electronica Sinia*, 2001, 29(6): 1–4.

[29] Chen V C. Analysis of micro-Doppler signature[J]. *IEE Proceeding-Radar, Sonar and Navigation*, 2003, 150(4): 271–276.

[30] Sparr T and Krane P. Micro-Doppler analysis of vibrating targets in SAR[J]. *IEE Proceeding-Radar, Sonar and Navigation*, 2003, 150(4): 277–283.

Deng Dong-hu (1986–) was born in Henan, China. He received the M.S. degree in electrical engineering from the Institute of Telecommunication Engineering, Air Force Engineering University (AFEU), Xi'an, China, in 2009. He is currently working toward his Ph.D. degree in the Radar and Signal Processing Laboratory, Institute of Information & Navigation, AFEU. His research interests include signal processing in ISAR.
E-mail: dengdonghu@163.com.

Zhang Qun (1964–) was born in Shaanxi, China. He received the M.S. degree in mathematics from Shaanxi Normal University, Xi'an, China, in 1988 and the Ph.D. degree in electrical engineering from Xidian University, Xi'an, in 2001. He was a Research Engineer from 2001 to 2003 and a Research Fellow from 2005 to 2006 with the Department of Electrical and Computer Engineering, National University of Singapore, Singapore. He is currently a Professor with the Institute of Information & Navigation, Air Force Engineering University, Xi'an, and an Adjunct Professor with the Laboratory of Wave Scattering and Remote Sensing Information, Fudan University, Shanghai, China. He has authored more than 200 papers on journals and conference proceedings. His research interests include signal processing, clutter suppression, and its application in SAR and ISAR.

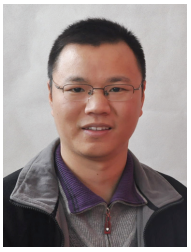

Luo Ying (1984–) was born in Hunan, China. He received the M.S. degree in electrical engineering, in 2008, from the Institute of Telecommunication Engineering, Air Force Engineering University (AFEU), Xi'an, China, where he is currently working toward the Ph.D. degree in electrical engineering. He is currently instructor with the Radar and Signal Processing Laboratory, Institute of Information & Navigation, AFEU. His research interests include signal processing and ATR in SAR and ISAR.